optics

MDPI

Article

Nature of Photoelectric Effect in a Ge-on-Si SPAD at Ultralow Energy in Incident Pulsed Laser Radiation

Valeri I. Kovalev [1,2]

[1] P. N. Lebedev Physical Institute of the Russian Academy of Sciences, Leninsky pr. 53, 119991 Moscow, Russia; v.kovalev@hw.ac.uk

[2] David Brewster Building, School of Engineering and Physical Sciences, Heriot-Watt University, Edinburgh EH14 4AS, UK

Abstract: The photoelectric effect in a *Ge*-on-*Si* single-photon avalanche detector (SPAD) at an ultralow energy in incident pulsed laser radiation is considered in the frame of the classical theory of the electrodynamics of continuous media. It is shown that the energy of incident laser radiation which is shared among a huge number of electrons in a *Ge* matrix can concentrate on only one of these through the effect of the constructive interference of the fields re-emitted by surrounding electrons. Conservation of energy in this case is upheld because of a substantial narrowing of the effective bandgap in heavily doped p-*Ge*, which is used in the design of the SPAD considered.

Keywords: photoelectric effect; sub-photon energy; classical electrodynamics; laser radiation; interference; heavily doped semiconductors

check for updates

Citation: Kovalev, V.I. Nature of Photoelectric Effect in a Ge-on-Si SPAD at Ultralow Energy in Incident Pulsed Laser Radiation. *Optics* **2021**, *2*, 45–53. https://doi.org/10.3390/opt2010004

Received: 12 April 2020
Accepted: 28 January 2021
Published: 31 January 2021

1. Introduction

Metrology of extremely low radiation energies/powers is the subject of vital importance for R&D in the area of quantum technologies, which include quantum communications [1] using quantum key distribution [2,3], secret sharing [4], cryptography [5] protocols, quantum computing [6] and quantum information processing [7]. It also secures progress in more classical technologies [8] such as deep space communications [9], telecommunications [10], sensing [11], rangefinding, light detection and ranging (LiDAR) [12] and depth imaging of objects [13], including imaging through various densities of different obscurants [14] and even covert imaging [15] applications. Single-photon detectors (SPD) are the devices that do the job. Significant advances in both photoelectric and thermal SPDs have been achieved in recent years [16–22]. As was conventionally happening in the history of science and technologies, the more objects of study and more research involved, the higher probability to find something new and unexpected. In the case of SPDs, such news is that their detection efficiency (DE) can be nonzero when the energy in a pulse of incident laser radiation W_i is less or even much less than the energy of the photon $\hbar\omega$ corresponding to the frequency ω of this radiation [19–22]. Such observations are in clear contradiction with Einstein's quantum model of the photoelectric effect (PE) [23], which states that a photoelectron appears when the electron absorbs from light the energy of a quantum $\hbar\omega$, i.e., of a photon, which exceeds the work function P or bandgap E_g of a material. This, in essence, a conservation of the energy condition in PE, presumes that the energy of a light pulse W_i, which is transferred to an electron in a medium, has to be not less than P or E_g and $\hbar\omega$. While for the superconductor SPDs [7], in which the energy gap $E_g \equiv 2\Delta << \hbar\omega$, the appearance of a photoelectron when $W_i << \hbar\omega$ does not contradict the conservation of energy law, in the case of photoelectric SPDs [19–21], in which it is presumed that $E_g \leq \hbar\omega$, such observations look surprising. In this work, a plausible explanation for such observations in *Ge*-on-*Si* single-photon avalanche diode (SPAD) detectors is given in the frame of the classical electrodynamics of continuous media. Active R&D interest in such detectors is high [15,20,21,24] because they are sensitive in

the near infrared, up to wavelengths of 1600 nm, they operate near room temperature and they are Si CMOS-compatible devices. As a consequence, the amount of data on their characteristics available for their theoretical analysis is high.

2. Device Design and Characteristics

The structure of the SPAD used in [20,21] is presented in Figure 1. The authors presume that an incident light, which enters the detector through a high-concentration boron-doped ($\sim 5 \times 10^{19}$ cm^{-3}) p++*Ge* (p-*Ge*) layer of thickness $l = 0.1$ μm, is absorbed with the creation of electron–hole pairs in a 1 μm-thick layer of intrinsic *Ge* (i-*Ge*). The created PEs are then dragged by an applied voltage of ~40 V toward the intrinsic *Si* (i-*Si*) layer of 1 μm thickness. In this layer, these PEs initiate an electron avalanche, which multiplies the number of electrons at the output of this layer to a readily detectable level. The *p*-doped *Si* of 0.1 μm thickness forms the charge sheet. It ensures that the electric field in i-*Ge* layer is well below an avalanche breakdown field, while the field in the *Si* multiplication layer is 3 times greater than the breakdown field to provide impact ionization. The structure was grown on a highly doped n++*Si* substrate. The material in i-*Ge* and i-*Si* layers is "pure", i.e., not intentionally doped, that is, with a concentration of uncontrolled admixtures of ~10^{15} cm^{-3}. The device with a 25 μm entrance aperture diameter operated at temperatures of $T = 100$–150 K. That SPAD was irradiated by a 10 kHz sequence of 50 ps pulses of laser radiation at wavelengths of $\lambda = 2\pi c/\omega = 1.31$ or 1.55 μm. The radiation from a laser was sent to the entrance of the detector through a single mode fiber (core diameter of~10 μm), a calibrated optical attenuator and a two-lens imaging system. This system allowed reducing the energy in each incident pulse W_i up to $\sim 0.01\hbar\omega \cong 10^{-21}$ J. The illuminated volume of *Ge* layers was estimated as $V \approx 1.1$ μm $\times$ (10 μm)$^2 \approx 10^{-10}$ cm^3. With such a SPAD, DE at $W_i \leq 0.1\hbar\omega$ was measured to be nonzero at both λ (~4% at $\lambda = 1.31$ μm and $T = 100$ K, and ~0.15% at $\lambda = 1.55$ μm and $T = 150$ K) [20]. The measured dependence of DE on W_i at $\lambda = 1.31$ μm and $T = 125$ K, by the authors [21], is presented in Figure 2. As can be seen, DE(W_i) saturates at ~100% when $>10\hbar\omega$ and linearly decreases to ~0.1% at $\sim 0.01\hbar\omega$ with ~13% at $\sim\hbar\omega$ (see Figure 2). In doing so, DE(W_i) does not manifest any peculiarities at $W_i \cong 1\hbar\omega$, which may be expected according to Einstein's model [23]. To elucidate the nature of such observations, we first looked more carefully to [23].

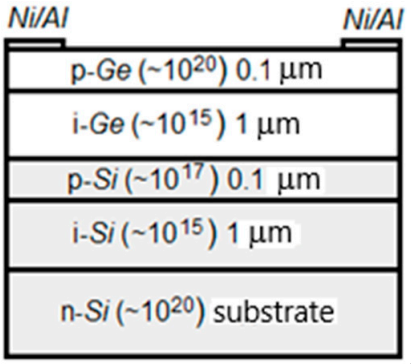

Figure 1. *Ge*-on-*Si* single-photon avalanche diode (SPAD) structure cross-section illustrating two *Ge* layers, two *Si* layers, *Si* substrate, *Ni/Al* contacts, doping number densities in cm^{-3} (in brackets) and layer thicknesses.

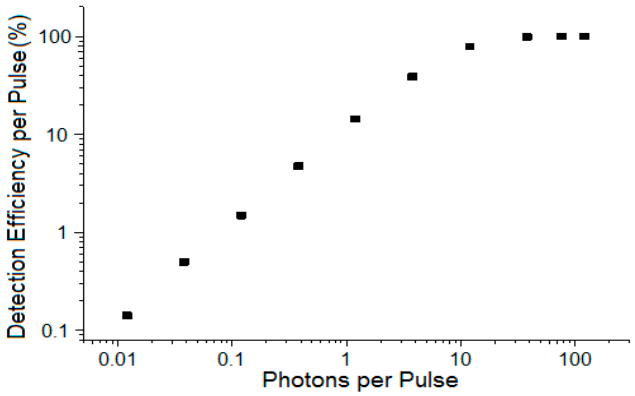

Figure 2. Detection efficiency (DE) vs. the energy in an incident radiation pulse.

3. Discussion

Analysis of the data presented above has led us to the following questions:

- To what extent is Einstein's model of PE relevant to the processes in such SPADs and observed results?
- If not Einstein's model, then how can the observed results and their interpretation be made compatible?

3.1. Einstein's Model and Its Prerequisites

According to Einstein [23], an electron, which is bound in a medium, becomes a photoelectron when its kinetic energy, acquired from incident radiation, is higher than the energy binding it to the medium. The incident radiation of frequency ω is considered as a flow of quanta with energy $\hbar\omega$. The important prerequisites of his model may be re-formulated as (1) the quanta penetrate to the surface layer of a material, where their energy is converted to the kinetic energy of electrons, and (2) one light quantum gives up all its energy to one electron.

Regarding these prerequisites in relation to detection of a single photon in SPADs, the first one requires that in the region of where a photoelectron is generated, incident radiation, i.e., the energy of a photon, is not attenuated due to its conversion to any other forms of energy, e.g., to heat, radiation of other frequencies. The objective data on the light absorption coefficient (α) in *Ge* show that this requirement is not met: at $\lambda \approx 1.3$–1.55 μm $\alpha = (5 \pm 1) \times 10^3$ cm^{-1} in i-*Ge* [25] and ~(1-2) $\times 10^3$ cm^{-1} in heavily doped p-*Ge* (concentration $N_p \geq 5 \times 10^{19}$ cm^{-3}) [26]. It follows from these data that, while the p-*Ge* layer is practically transparent ($\alpha l \leq 0.02$), the i-*Ge* layer is half transparent ($\alpha l \cong 0.5$). This means, in particular, that if a photoelectron appears in the i-*Ge* layer, it, most probably, happens in a thin entrance surface part ($l < 0.1$ μm) of the whole i-*Ge* layer. This may also happen in the p-*Ge* layer.

To choose between the two, we must take into account the following circumstances. It is known that conventional i-*Ge* is a nondegenerate semiconductor with a residual concentration of uncontrolled admixtures and defects of ~10^{15} cm^{-3}. In such material, the energy gap, E_g, between the valence and conduction bands at $T \approx 100$–150 K is of ~0.7 eV, and the Fermi energy level is located in roughly the middle of the forbidden zone, $F \cong E_g/2$. Accordingly, the temperature-induced concentration of free electrons $N_e(T)$ in the conduction band of an i-*Ge*, which is expected to be of <10^4 cm^{-3} (at $T < 150$ K) [27], is negligible compared to $N_e \cong 10^{15}$ cm^{-3} due to uncontrolled admixtures and defects [28]. It then follows that in the volume of i-Ge layer in [20,21], $V \approx 1$ μm $\times$ (10 μm)$^2 \approx 10^{-11}$ cm^3, the number of free electrons will be of ~10^5. Obviously, it is problematic to detect the appearance of a single PE on such a background.

The situation is different in a heavily doped p-*Ge* ($N_p \cong (0.5$–$1) \times 10^{20}$ cm^{-3}) [27]. The Fermi level in such a case is shifted to the valence band and all free electrons are captured by acceptors. As a result, N_e tends to zero. In this case, the appearance of a single

additional free electron is obviously an event. If this is the case, the SPAD we consider operates like a conventional photomultiplier tube (PMT), in which the p-*Ge* layer plays the role of a photocathode, and the i-*Ge* layer is equivalent to the vacuum spacing between the photocathode and the multiplying electrons system of dynodes. Such a role of p-*Ge* and i-*Ge* layers in SPADs was never discussed before.

It follows from above that the p-*Ge* layer is transparent for incident light ($\alpha l < 0.02$) and has a low concentration of free electrons. A material in which such conditions are upheld behaves as an optically transparent dielectric.

3.2. The Electromagnetic Energy in a Dielectric

According to [29], the density of electromagnetic (EM) energy, U_d, in a dielectric medium ($\mu = 1$) is

$$U_d = \frac{1}{8\pi}\left(\varepsilon E_d^2 + H_d^2\right) \equiv \frac{1}{8\pi}\left(E_d^2 + H_d^2 + 4\pi\chi E_d^2\right) \quad (1)$$

where E_d and H_d are the amplitudes of electric and magnetic fields, $\varepsilon = 1 + 4\pi\chi$ is the permittivity and χ is the susceptibility. The last term in (1) is the part of the EM energy density which is transferred to the movement of the bound electrons (BEs) in a dielectric. It is important to note here that in absence of other losses, this energy returns to the radiation field when it leaves a medium. Dividing this energy by the density of the BEs number, N_e, which are involved in the interaction, one can get the amount of EM energy, which is transferred to one BE, W_1. To estimate W_1 in the case under consideration, we must take into account that the permittivity of *Ge* is $\varepsilon \cong n^2 \cong 17$. This, in particular, means that, to sufficient, accuracy we can suppose that $U_d \cong U_{in} = I_{in}/c$, where I_{in} is the intensity of incident laser radiation in vacuum ($n = 1$), i.e., before it enters the SPAD, in each pulse and c is the velocity of light in vacuum. To estimate I_{in} and U_d, respectively, we take, for definiteness, the energy in each pulse of $0.1\hbar\omega \cong 1.5 \times 10^{-20}$ J and the diameter of the irradiated spot at the entrance of the device of 10 μm. Then, for a 50 ps duration of pulses, we get $I_{in} \cong 0.4$ mW/cm^2 and $U_d \cong 10^5$ eV/cm^3. Therefore, taking into account that the total density of BEs in *Ge*, defined as N_e, = N_a x32 is $\approx 1.3 \times 10^{24}$ cm^{-3}, where N_a is the number of *Ge* atoms per cm^3, which is ~4×10^{22} cm^{-3}, and "32" is the number of electrons in a *Ge* atom, we get $W_1 \cong 10^{-19}$ eV. This energy is obviously much, much less than the conventional direct bandgap energy in *Ge*, e.g., E_g(125K) $\cong$ 0.7 eV. This is actually true even for radiation pulses with energy of $1s\hbar\omega$, $10s\hbar\omega$, $1000s\hbar\omega$, etc.

Then, the following questions need answers: (1) How can only one of all electrons in the irradiated p-*Ge* layer get the whole energy from an incident radiation pulse? (2) Why does that electron overcome the bandgap energy barrier presumed to be E_g(125K) $\cong$ 0.7 eV when the energy it can get from a pulse is much less than E_g?

3.3. The Effect of Interference

To answer the first question, we must account for the fact that an electron driven by an oscillating electric field is the source of a secondary emission. Interference is the only physical phenomenon which is capable of redistributing the averaged energy in a system of many radiation emitters. If we then take into consideration that the incident radiation, which is generated by a laser, is highly coherent throughout the volume of *Ge* layers, $V \approx 10^{-10}$ cm^3, the driven oscillations of electrons in this volume and the fields reradiated by each of them will be coherent. As such, re-radiated fields can constructively interfere at some time during irradiation and at some point inside this volume (see, e.g., point C in Figure 3). Taking into account that the total density number of electrons in *Ge* is $N_e \approx 1.3 \times 10^{24}$ cm^{-3}, then the number of electrons, involved in such an interaction, is $N \cong N_e \times V \approx 1.4 \times 10^{14}$, and potentially the factor of radiation intensity, and EM energy density, enhancement may be potentially up to $N^2 \approx 2 \times 10^{28}$. It is much less in reality.

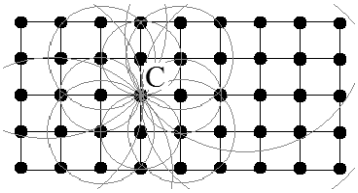

Figure 3. Schematic sketch of how the constructive interference of electromagnetic (EM) fields, which are re-emitted by surrounding electrons, may increase the radiation intensity at point C in a material lattice. Thin circles represent the wavefronts of re-emitted fields.

To estimate a potential factor of enhancement, we must take into consideration several circumstances. Firstly, the nature of secondary emission by electrons is twofold: it may be a result of accelerated movement of an electron [30] and of an oscillating dipole which is formed by an electron and a positively charged atomic rest [29].

In the first case, all ~1.3×10^{24} cm^{-3} electrons of a material are sources of re-emission because the electric field E_i of the incident radiation moves an electron regardless of where it is located. The strength (amplitude) of an electric field, E_e, that is re-emitted by being driven with the acceleration $\dot{v}$ electron decreases with distance R from that electron as [30]

$$E_e = \frac{e\,\dot{v}}{c^2 R}\sin\theta \tag{2}$$

where θ is the angle between the direction of the Hertzian vector and the direction of the observation. Correspondent movement is governed by the equation

$$\dot{v} = \frac{e}{m}E_i e^{-i\omega_0 t} \tag{3}$$

where $\dot{v}$ is the velocity of an electron, e and m are its charge and mass and E_i is the amplitude of the electric field of the incident radiation of frequency ω_0. Accordingly, we have for the re-emitted field amplitude at the distance R from a point charge emitter

$$E_e = \frac{e^2 E_i}{mc^2 R}\sin\theta \tag{4}$$

In the second case, an atom is considered as a set of dipole oscillators. These re-emit an EM wave to the electric field, the amplitude of which is decaying with R as [29]

$$E_d = er(t)\left(\frac{1}{R^3} + i\frac{\omega_0}{sR^2} - \frac{\omega_0^2}{c^2 R}\right)\sin\theta \cong -er(t)\frac{\omega_0^2}{c^2 R}\sin\theta \tag{5}$$

where $r(t)$ is the displacement of an electron from its equilibrium position at an orbit in an atom, which is driven by the electric field of the incident radiation E_i. This displacement may be described by the oscillator equation [31]

$$\ddot{r} + \gamma_i \dot{r} + \omega_g^2 r = \frac{e}{m}E_i e^{-i\omega_0 t} \tag{6}$$

where γ_i is the coefficient, which characterizes a loss of oscillation energy due to inelastic collisions of an electron with surrounding particles and the material lattice, and ω_g is the resonant frequency of an oscillator, the magnitude of which is determined by a bounding force between an electron and its atomic rest. When the radiation is monochromatic, a solution to Equation (6) is

$$r_a = \frac{eE_i}{m(\omega_g^2 - \omega_0^2 - i\gamma_i\omega_0)} \tag{7}$$

It follows from Equation (7) that, since $\gamma_i << \omega_g$, r_a maximizes when $\omega_0 = \omega_g$ and decreases proportionally to $1/{\omega_g}^2$ when $\omega_g >> \omega_0$. It then follows from Equation (7) that

the dipole-kind re-emission by the electrons, which occupy the deeper orbits, may be considered negligible since these have much higher energies than those bound with an atomic rest, i.e., much higher ω_g. Consequently, in a *Ge* atom, the number of BEs, which are active in the dipole-kind interaction with NIR optical radiation, is limited to 4, giving the density of correspondent Bes, $N_d = 4N_a \approx 1.6 \times 10^{23}$ cm^{-3}.

Let us evaluate the effect of the coherent summation at some point, C, in the p-*Ge* layer of the fields re-emitted by all involved electrons and dipoles in the SPAD. Consider in a medium a half-sphere of radius R with the thickness of wall δR. Its volume is

$$\delta V = \frac{2}{3}\pi\left[(R+\delta R)^3 - R^3\right] \cong 2\pi R^2 \delta R \quad (8)$$

The number of emitters in this volume is

$$\delta N_{e,d} = N_{e,d}\delta V \cong 2\pi N_{e,d} R^2 dR \quad (9)$$

All these emitters are equidistant from some point, C, in the p-*Ge* layer (see Figure 4). An effective distance R_m in the body of the SPAD, from which a re-emitted radiation may have an essential magnitude at C, is of α^{-1}. We then must account for the notion that the electric field of the incident radiation E_i drives the emitters in the plane parallel to the p-*Ge* layer. These emitters give rise to a re-emission of radiation with the electric field amplitude E_e dependent on θ (see Equations (4) and (5)). To account for this effect, we choose on the semi-sphere layer of a radius R a sub-volume $\delta v = \delta s \delta R = R^2 \delta\theta\delta\varphi\delta R$, where δs is the cross-sectional area of the sub-volume. All emitters in such a volume will produce at C the fields of practically the same amplitude.

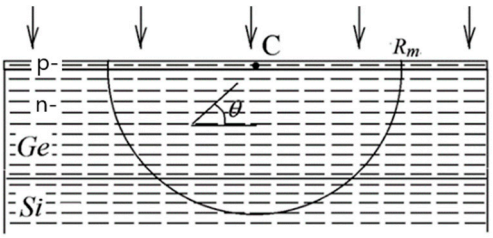

Figure 4. Schematic sketch of the *Ge* (p- and n-) and *Si* layers in a SPAD, the re-emission from which contributes to an enhanced field at the point C in the p-*Ge* layer. Vertical arrows represent the propagation direction of the incident radiation, horizontal dashes represent electrons driven by the incident radiation, R_m is the effective absorption length of radiation and θ is the angle between the direction of electron oscillations and the direction from this electron to point C.

Multiplying δv by N_e and E_e from Equation (4) and integrating over R, θ and φ, we get the field, which may be induced at point C by the coherent summation of the fields re-emitted by all electrons in *Ge* and *Si* layers in the SPAD:

$$E_{e\Sigma} = E_i \frac{\pi N_e e^2}{mc^2}\left(R_m^2 - a_0^2\right) = E_i F_e(R_m) \quad (10)$$

where $a_0 \cong 2.8 \times 10^{-8}$ cm is the *Ge/Si* lattice constant. The magnitude of $|F_e(R_m)|^2$ determines a magnitude of W_1 enhancement at point C when re-emission of all electrons in the irradiated volume is coherently summed. Substituting into Equation (10) the magnitudes of the corresponding parameters of Ge and Si ($N_e \approx 10^{24}$ cm^{-3}, $n_{Ge} \cong 4{,}1$, $n_{Si} \cong 3.5$ and $R_m \cong \alpha^{-1} \cong 2$ μm), one would get $|F_e|^2 \cong 2 \times 10^9$, which is clearly much less than the desirable ~10^{19}.

Similarly, using Equations (5) and (7), presuming $\omega_0 = \omega_g$ and taking into account that $R_m >> a_0$, we get the enhancement factor in the case of re-emission by dipoles:

$$|F_d|^2 \cong \left[\frac{\pi N_d e^2 \omega_g}{mc^2 \gamma_i} R_m^2\right]^2 \tag{11}$$

Among the parameters, magnitudes of which determine $|F_d|^2$, the most uncertain one is γ_i. According to [30] its magnitude in semiconductors may vary in the range from ~10^{10} s^{-1} at a room temperature to ~10^7 s^{-1} at lower T. Substituting to Equation (11) magnitudes of e, m, n, c and $\omega_g = E_g/\hbar = 10^{15}$ s^{-1}, we get

$$|F_d|^2 \approx \left(\frac{6 \times 10^{18}}{\gamma_i}\right)^2 \tag{12}$$

It follows from Equation (12) that at $\gamma_i \leq 2 \times 10^9$ s^{-1}, which is a reasonable magnitude for *Ge* at T = 100–150 K, $W_1|F_d|^2 \geq 0.7$ eV, even at $W_1 = 0.01\hbar\omega_0 \cong 10^{-21}$ J, i.e., this is just the energy sufficient for an electron to overcome the energy barrier of the forbidden zone in *Ge*. An important condition for the realization of such enhancement, which is $\omega_0 = \omega_g$, is the well-known Einstein condition $\hbar\omega_0 = E_g = \hbar\omega_g$.

The only problem, however, is that the conservation of energy in the case under consideration remains an enigma when $W_i < E_g$. A specific feature of heavily doped semiconductors, which is p-*Ge* used in SPADs [20], gives a clue for resolving this issue.

3.4. The Bandgap in a Heavily Doped p-Ge

In such materials, the typical for intrinsic semiconductors' sharp zone boundaries (dashed straight lines in Figure 5a) is blurred and the "tails" of the allowed occupation states penetrate the forbidden zone, resulting in a substantially narrower effective bandgap E_{ge}. [27]. The physical reason for this effect is the local fluctuations of the internal electric field in a material due to a generic inhomogeneity of the spatial distribution of a dopant at its high concentration [32]. The local shift of zone boundaries, which is induced by such fluctuations, is illustrated in Figure 5a by the two solid lines and the dashed curved lines. A deformation of zone boundaries, which is schematically depicted by two parallel solid lines, is typical for the case when the effective masses of charge carriers at zone boundaries coincide [27]. The local bandgap in this case does not change. As shown in [32], such a case takes place in p-*Ge* for indirect interband transitions. The radiation with λ = 1.31 μm ($\hbar\omega_0 \cong 0.85$ eV) falls in the range of direct transitions in *Ge* ($E_{gd} \cong 0.85$ eV). Since an effective mass of electrons at the center of the Brillouin zone is much less than that of holes, the amplitude of the conduction zone boundary deformation is essentially reduced [32] (the dashed curve). The shaded areas represent the "tails", which are a result of averaging the field fluctuations. Figure 5b illustrates, schematically, the averaged densities of the allowed occupation states $N_{c,v}(E)$ for electrons (c) and holes (v) for intrinsic (dash-dotted lines) and for highly doped (solid lines) material, and the intrinsic E_{gi} and effective bandgap E_{ge}.

In particular, in *Ge* at $N_d \geq 10^{20}$ $см^{-3}$, the factor of the effective gap narrowing may be up to ~100 [27]. These circumstances allow us to account for why the appearance of a photoelectron resulting from the irradiation of a light pulse with sub-photon energy in the SPAD under consideration does not contradict the conservation of the energy principle in this interaction.

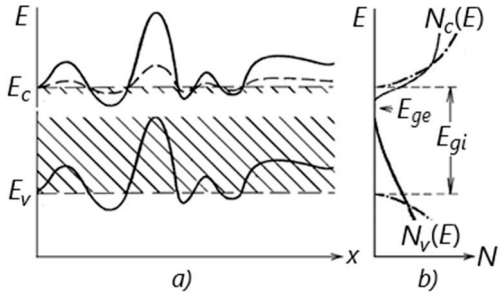

Figure 5. (**a**) Spatial variation in the conduction and valence band boundaries, $E_{c,v}$, in a pure semiconductor (dashed straight lines) and in a heavily doped semiconductor (solid lines). (**b**) Effective densities of the allowed occupation states $N_{c,v}(E)$ for electrons (c) and holes (v) for intrinsic (dash-dotted lines) and for highly doped (solid lines) material.

4. Conclusions

Classical macroscopic electrodynamics allows us to account for the photoelectric effect in a *Ge*-on-*Si* SPAD when the incident pulsed laser radiation is of sub-photon energy. The energy of the incident laser radiation, when transferred to a huge number of electrons in the *Ge* matrix, can concentrate on only one of these through the effect of constructive interference of the fields re-emitted by surrounding electrons. The conventional necessary condition for the photoelectric effect in a material, which reads as $\omega_0 = E_g/\hbar$ [23], comes to the model as a resonant condition for the Lorentz classical oscillator model. The conservation of the energy law in this interaction is upheld because of a substantial narrowing of the effective bandgap in the heavily doped p-*Ge* layer of the SPAD. Since the classical model presented in this work is linear with respect to the energy in an incident pulse W_i, the fact that the experimental data shown in Figure 2 demonstrate a smooth linear decrease in the detection efficiency with a decrease in W_i when $W_i < 10\ \hbar\omega$ and manifest no peculiarities at $W_i \cong 1\ \hbar\omega$ is in good agreement with the developed model.

Funding: This research received no external funding.

Acknowledgments: The author would like to thank G. S. Buller and P. Vines for useful discussions.

Conflicts of Interest: The author declares no conflict of interest.

References

1. Zhang, J.; Itzler, M.A.; Zbinden, H.; Pan, J.-W. Advances in InGaAs/InP single-photon detector systems for quantum communication. *Light Sci. Appl.* **2015**, *4*, e286. [CrossRef]
2. Takesue, H.; Nam, S.W.; Zhang, Q.; Hadfield, R.H.; Honjo, T.; Tamaki, K.; Yamamoto, Y. Quantum key distribution over a 40-dB channel loss using superconducting single-photon detectors. *Nat. Photonics* **2007**, *1*, 343–348. [CrossRef]
3. Buller, G.S.; Warburton, R.E.; Pellegrini, S.; Ng, J.S.; David, J.P.R.; Tan, L.J.J.; Krysa, A.B.; Cova, S. Single-photon avalanche diode detectors for quantum key distribution. *IET Optoelectron.* **2007**, *1*, 249–254. [CrossRef]
4. Xiao, L.; Long, G.L.; Deng, F.G.; Pan, J.W. Efficient multiparty quantum-secret-sharing schemes. *Phys. Rev. A* **2004**, *69*, 052307. [CrossRef]
5. Gisin, N.; Ribordy, G.; Tittel, W.; Zbinden, H. Quantum cryptography. *Rev. Mod. Phys.* **2002**, *74*, 145–195. [CrossRef]
6. O'Brien, J.L. Optical quantum computing. *Science* **2007**, *318*, 1567–1570. [CrossRef] [PubMed]
7. Wang, J.; Sciarrino, F.; Laing, A.; Thompson, M.G. Integrated photonic quantum technologies. *Nat. Photonics* **2019**, *14*, 273–284. [CrossRef]
8. Hall, D.; Liu, Y.-H.; Lo, Y.-H. Single photon avalanche detectors: Prospects of new quenching and gain mechanisms. *Nanophotonics* **2015**, *4*, 397–412. [CrossRef]
9. Hemmati, H.; Biswas, A.; Djordjevic, I.B. Deep space optical communications: Future perspectives and applications. *Proc. IEEE* **2011**, *99*, 2020–2039. [CrossRef]
10. Campbell, J.C. Recent advances in telecommunications avalanche photodiodes. *J. Lightwave Tech.* **2007**, *25*, 109–121. [CrossRef]
11. Niclass, C.; Rochas, A.; Besse, P.-A.; Charbon, E. Design and characterization of a CMOS 3-D image sensor based on single photon avalanche diodes. *IEEE J. Solid State Circuits* **2005**, *40*, 1847–1854. [CrossRef]

12. Warburton, R.E.; McCarthy, A.; Wallace, A.M.; Hernandez-Marin, S.; Hadfield, R.H.; Nam, S.W.; Buller, G.S. Subcentimeter depth resolution using a single-photon counting time-of-flight laser ranging system at 1550 nm wavelength. *Opt. Lett.* **2007**, *32*, 2266–2268. [CrossRef] [PubMed]
13. Pawlikowska, A.M.; Halimi, A.; Lamb, R.A.; Buller, G.S. Single-photon three-dimensional imaging at up to 10 kilometers range. *Opt. Express* **2017**, *25*, 11919–11931. [CrossRef] [PubMed]
14. Tobin, R.; Halimi, A.; McCarthy, A.; Laurenzis, M.; Christnacher, F.; Buller, G.S. Three-dimensional single-photon imaging through obscurants. *Opt. Express* **2019**, *27*, 4590–4611. [CrossRef]
15. Llin, L.F.; Kirdoda, J.; Thorburn, F.; Huddleston, L.L.; Greener, Z.M.; Kuzmenko, K.; Vines, P.; Dumas, D.C.S.; Millar, R.W.; Buller, G.S.; et al. High sensitivity Ge-on-Si single-photon avalanche diode detectors. *Opt. Lett.* **2020**, *45*, 6406–6409. [CrossRef]
16. Hadfield, R.H. Single-photon detectors for optical quantum information applications. *Nat. Photonics* **2009**, *3*, 696–705. [CrossRef]
17. Buller, G.S.; Collins, R.J. Single-photon generation and detection. *Meas. Sci. Technol.* **2010**, *21*, 012002. [CrossRef]
18. Eisaman, M.D.; Fan, J.; Migdall, A.; Polyakov, S.V. Invited Review Article: Single-photon sources and detectors. *Rev. Sci. Instrum.* **2011**, *82*, 071101. [CrossRef]
19. Kang, Y.; Lo, Y.-H.; Bitter, M.; Kristjansson, S.; Pan, Z.; Pauchard, A. InGaAs-on-Si single photon avalanche photodetectors. *Appl. Phys. Lett.* **2004**, *85*, 1668–1670. [CrossRef]
20. Warburton, R.E.; Intermite, G.; Myronov, M.; Allred, P.; Leadley, D.R.; Gallacher, K.; Paul, D.J.; Pilgrim, N.J.; Lever, L.J.M.; Ikonic, Z.; et al. Ge-on-Si Single-Photon Avalanche Diode Detectors: Design, Modeling, Fabrication, and Characterization at Wavelengths 1310 and 1550 nm. *IEEE Trans. Electron Devices* **2013**, *60*, 3807–3813. [CrossRef]
21. Vines, P.; Kuzmenko, K.; Kirdoda, J.; Dumas, D.C.S.; Mirza, M.M.; Millar, R.W.; Paul, D.J.; Buller, G.S. High performance planar germanium-on-silicon single-photon avalanche diode detectors. *Nat. Commun.* **2019**, *10*, 1086. [CrossRef] [PubMed]
22. Gol'tsman, G.N.; Okunev, O.; Chulkova, G.; Lipatov, A.; Semenov, A.; Smirnov, K.; Voronov, B.; Dzardanov, A.; Williams, C.; Sobolewski, R. Picosecond superconducting single-photon optical detector. *Appl. Phys. Lett.* **2001**, *79*, 705–707. [CrossRef]
23. Einstein, A. Uber einen die Erzeugung und Verwandlung des Lichtes betreffenden heuristischen Gesichtspunkt. *Ann. Phys.* **1905**, *17*, 132–148. [CrossRef]
24. Kirdoda, J.; Dumas, D.C.S.; Kuzmenko, K.; Vines, P.; Greener, Z.M.; Millar, R.W.; Mirza, M.M.; Buller, G.S.; Paul, D.J. Geiger Mode Ge-on-Si Single-Photon Avalanche Diode Detectors. In Proceedings of the 2019 IEEE 2nd British and Irish Conf. on Optics and Photonics (BICOP), London, UK, 11–13 December 2020. [CrossRef]
25. Dash, W.; Newman, R. Intrinsic optical absorption in single-crystal germanium and silicon. *Phys. Rev.* **1955**, *99*, 1151–1155. [CrossRef]
26. Bagaev, V.S.; Proshko, G.P.; Shotov, A.P. Infrared absorption in heavily doped germanium. *Sov. Phys. Solid State* **1963**, *4*, 2363–2368.
27. Bonch-Bruevich, V.L.; Kalashnikov, S.G. *Physics of Semiconductors*; Nauka Press: Moscow, Russia, 1977. (In Russian)
28. Cuttris, D.B. Relation Between Surface Concentration and Average Conductivity in Diffused Layers in Germanium. *Bell Syst. Tech. J.* **1961**, *40*, 509–523. [CrossRef]
29. Tamm, I.E. *Basics of Electricity Theory*; OGIZ: Moscow, Russia, 1946. (In Russian)
30. Jackson, J.D. *Classical Electrodynamics*, 3rd ed.; Willey & sons: New York, NY, USA, 1962.
31. Lorentz, H.A. *The Theory of Electrons and its Applications to the Phenomena of Light and Radiant Heat*; Leipzig B.G.: Teubner, Germany, 1916.
32. Keldish, L.V.; Proshko, G.P. Infrared absorption in heavily doped germanium. *Sov. Phys. Solid State* **1964**, *5*, 2481–2488.